

# Improvements to a GPS Radio Occultation Ray-tracing Model and Their Impacts on Assimilation of Bending Angle

H. Liu and X. Zou<sup>1</sup>

Florida State University, Tallahassee, Florida, USA

*(Submitted to J. G. R.)*

*(Revised submitted on March 7, 2003)*

---

<sup>1</sup>Corresponding author: X. Zou, Department of Meteorology, Florida State University, Tallahassee, 404  
Love Bldg., FL 32306-4052, USA. Phone: (850) 644-6025, Email: zou@met.fsu.edu

## Abstract

Several efforts are made to improve the accuracy and efficiency of a 2D GPS radio occultation forward ray-tracing model. First, a large impact parameter offset existed in the forward model, caused by the inconsistency in the definition of the “occultation point” between the forward model and the GPS/MET data. The forward model is modified to be consistent with the GPS/MET data. Second, the errors in the simulation of the impact parameter and the bending angle due to the original starting point scheme of the ray integration are examined and a new starting point scheme is introduced to reduce the forward modeling errors. Third, to more accurately simulate the GPS/MET bending angle data, a derivation of the bending angle from a Doppler shift measurement under the application of Snell’s law is incorporated into the ray-tracing model. Fourth, a variable step size for the ray integration is proposed to the forward ray-tracing model to reduce its computational cost.

Assessment of the impacts of these modifications to the forward modeling of the bending angle and to the data assimilation of the bending angle is carried out with simulated bending angles and impact parameters derived from an accurate 3D ray-tracing model. The 3D ray-tracing model simulates a total of 133 occultation profiles with the actual satellite positions and velocities taken from the 133 GPS/MET occultations observed on October 11, 1995. The NCEP analysis at T126L28 resolution is used to represent the “true” refractivity field of the atmosphere. The bending angles and impact parameters in the 3D ray-tracing model are derived following the same data processing procedure used in the GPS/MET experiment. All the input parameters (e.g., the tangent direction at the perigee point, etc.) required by the 2D ray-tracing model are provided by the 3D ray-tracing model. Numerical results with and without the above mentioned modifications to the 2D ray-tracing model are examined and

compared with the 3D ray-tracing model results and the NCEP T126L28 analysis. It is shown that the modifications to the 2D ray-tracing model significantly reduce the errors in the forward simulation of the bending angle and the impact parameter, and thus greatly improve the accuracy of the temperature, specific humidity, and surface pressure field analyses produced by GPS data assimilation, especially in middle and lower troposphere.

## 1 Introduction

Space-borne GPS occultation technology allows for measurements of the phase delay of a GPS radio signal. The phase delay is measured by GPS signal receivers on low earth orbiting (LEO) satellites. Information on the temperature, moisture, and surface pressure fields of the atmosphere are contained in these measurements. The GPS occultation technique was first demonstrated in the GPS/MET experiment [*Kursinski et al.*, 1996; *Ware et al.*, 1996]. Direct assimilation of the bending angles derived from the GPS phase delay measurements is likely the most appropriate way to extract useful temperature, moisture, and surface pressure information in the atmosphere [*Zou et al.*, 1999; *Kuo et al.*, 2000]. In order to assimilate GPS/MET bending angle observations, a 2D forward ray-tracing model and its tangent linear and adjoint models were developed and incorporated into the U. S. National Centers for Environmental Prediction (NCEP) statistical spectral interpolation (SSI) system [*Zou et al.*, 1999; *Zou et al.*, 2000]. Several numerical experiments using this system were carried out to assess the impacts of the GPS/MET bending angle observations on large-scale analyses and forecasts (Liu et al., 2001; Shao and Zou, 2002). These studies have shown that the assimilation of the GPS/MET bending angles improved the global analyses and forecasts of

temperature and specific humidity above 850 hPa. However, a systematic positive impact on the temperature and specific humidity analysis in the lower troposphere (below 850 hPa) and on the surface pressure field is still difficult to obtain. This could result from large forward model errors, the very limited number of the GPS/MET occultations available in the lower troposphere, and the larger observation errors in low troposphere<sup>2</sup>. In this study, we focus on reducing the forward model errors and examine their impact on GPS data assimilation.

Several simplifications were made in the original 2D forward ray-tracing model which was used for bending angle assimilation. Some of them could significantly contribute to the large errors of the model. For example, a simulated ray starts from a virtual GPS location, which was simply defined at a point about 20,200 km away from the observed perigee point along the tangent direction of the observed ray at the perigee point. This approximation may cause the modeled ray path go to pass below the observed ray perigee point, with a tangent direction not parallel to the observed tangent direction near the perigee point (with an angle of approximately half of the observed bending angle). When the simulated bending angle, as a function of the impact parameter, is interpolated to the observed perigee point, errors will arise. These errors are amplified in the lower troposphere where the bending of the ray is large. Another simplification in the original 2D model was associated with the derivation of the bending angle. In the GPS/MET and other experiments, the bending angle is derived from the Doppler shift measurement under the application of Snell's law, because the true refractivity of the atmosphere is not known and the spherical symmetry assumption has to

---

<sup>2</sup>The quantity and the quality of GPS observations in the lower troposphere from subsequent GPS occultation data sets (eg, CHallenging Minisatellite (CHAMP), SAC-C (Satelite Argentino de Observacion de la Tierra), Constellation Observing System for Meteorology, Ionosphere and Climate (COSMIC)) are expected to be significantly improved.

be used to derive the GPS bending angle. In the model, however, the ray was simulated by solving the ray equation based on the refractivity of the guess field, and the bending angle was taken as the difference of the ray tangent directions at the beginning and ending points of the rays. In order to simulate the GPS bending angle data more accurately, the forward model should follow the derivation of the observed bending angle as closely as possible, i.e., also applying Snell's law in the derivation of the simulated bending angle. The third example is to understand and to reduce the large impact parameter offset in the original ray-tracing model found in our previous study [*Liu et al.*, 2002]. Finally, the computational cost of the forward ray-tracing model must be reduced to meet future operational requirements. All of these issues will be studied in this paper.

The paper is organized as follows. In section 2, the cause for the large impact parameter offset will be identified. Then the deficiencies of the original starting point scheme for the ray integration will be discussed and a new starting point scheme will be introduced. The derivation of the bending angle using Snell's law is also incorporated into the forward ray-tracing model. In addition, a variable step size for the ray integration is adapted to increase the computational efficiency of the ray-tracing model. In section 3, data assimilation experiments incorporating 133 GPS/MET bending angle profiles are carried out using the modified and the original forward ray-tracing models and their corresponding adjoint operators. Impacts of assimilating the GPS bending angle data with and without these new modifications on the optimal solution of the temperature, moisture, and surface pressure fields are discussed. Conclusions are given in section 4.

## 2 Modifications to the 2D forward ray-tracing model

### 2.1 A brief description of the 2D forward ray-tracing model

Details of the 2D forward ray-tracing model and its tangent linear and adjoint operators were provided in *Zou et al.* [1999]. Only a brief description of the forward model is provided below to ease the discussions of the proposed modifications.

The propagation of electro-magnetic radiation, i.e., the GPS ray path, is governed by the following two coupled first order ray equations:

$$\begin{aligned}\frac{d\vec{x}}{d\tau} &= \vec{y}(\tau) \\ \frac{d\vec{y}}{d\tau} &= n\nabla n\end{aligned}\tag{1}$$

where  $\vec{x} = (x_1(\tau), x_2(\tau), x_3(\tau))$  is the Cartesian coordinate vector representing the ray trajectory parameterized with a parameter  $\tau$ ,  $d\tau = \frac{ds}{n}$ ,  $s$  is the length of the ray, and  $n$  is the atmospheric index of refraction. The simulated ray can be obtained by a numerical integration of Eq. (1) given the initial values of  $\vec{x}$  and  $\vec{y}$  at a starting point which approximates the GPS position. The modeling of the simulated bending angle is completed through the following procedures:

1. The tangent vector of the observed ray at the perigee point ( $\vec{u}_p^t$ ) is determined based on the observed perigee point location vector ( $\vec{x}_p$ ) and the unit vector normal to the occultation plane at the perigee point ( $\vec{u}_p^n$ ):

$$\vec{u}_p^t = \frac{\vec{x}_p}{|\vec{x}_p|} \times \vec{u}_p^n\tag{2}$$

2. A virtual GPS satellite position ( $\vec{x}_0$ ) was calculated, which was located in the opposite direction of the tangent vector ( $\vec{u}_p^t$ ) 20,200 km away from the perigee point:

$$\vec{x}_0 = \vec{x}_p - \lambda \vec{u}_p^t, \quad |\vec{x}_0 - \vec{x}_p| = |\lambda \vec{u}_p^t| = 20200 km \quad (3)$$

3. The initial direction of the simulated ray at the virtual GPS location was found by taking the tangent direction of the observed ray at the perigee point:

$$\vec{y}_0 = \vec{u}_p^t \quad (4)$$

4. The virtual LEO satellite position ( $\vec{x}_f$ ) was defined at a point on the ray whose distance to the earth's surface was greater than 100 km.
5. The angle between the tangent direction vector at the GPS position ( $\vec{u}_0^t$ ) and that at the LEO satellite position ( $\vec{u}_f^t$ ) was calculated as the ray bending angle:

$$\alpha(p) = (\widehat{\vec{u}_0^t, \vec{u}_f^t}) \quad (5)$$

where the hat  $(\widehat{\ , \ })$  represents the angle between the two vectors and  $p$  is the impact parameter at the LEO satellite location.

The 2D forward ray-tracing model is run at T126L28 resolution for the evaluation of the forward model in this section and at T62L28 resolution for the data assimilation experiments (Section 3). The T126L28 and T62L28 models have a horizontal resolution of approximately 0.9 and 1.9 degrees, respectively. Both models have the same 28 vertical layers, with a vertical resolution of about 0.4 km between the surface and 10 km, 2 km between 10 and 20 km, and 4 km between 20 and 40 km. The value of the bending angle in Eq. (5) as a function of the impact parameter at the LEO satellite position is compared with the observed bending angle as a function of the observed impact parameter.

The refractivity and its gradient, fields required by the forward ray-tracing model, can be calculated given a 3D distribution of temperature and specific humidity, and a 2D surface pressure field. From the Earth's surface to an altitude of 35 km, the NCEP analysis is used. Above 35 km, the Committee on Space Research International Reference Atmosphere (CIRA) data is used. Only the vertical gradient of the refractivity is used by the ray-tracing model. The ray-tracing is carried out in a 2D occultation plane, which is defined as a plane that contains the GPS and LEO satellite positions and the Earth's local curvature center.

The GPS bending angle measurements used in this study are generated through an accurate 3D ray-tracing model [Hoeg *et al.*, 1995]. In this model, the ray path that intersects both GPS and LEO satellites is found using a ray-shooting method through an iterative procedure. The expected accuracy at the ending point of the ray path, compared with the actual LEO satellite position, is within 1 mm. The satellite position vectors and velocities required by the 3D ray-tracing model are obtained from 133 observed GPS/MET occultation profiles from October 11, 1995. The 3D ray-tracing model uses the NCEP T126L28 analysis fields. The 3D model produces the phase delay for each simulated ray. Then the GPS/MET Level-3 processing software [Rocken *et al.*, 1997] is used to obtain the "observed" bending angle, impact parameter, perigee point position, tangent direction of the ray and the unit vector normal to the occultation plane at the perigee point. In the following experiments, each of the 133 occultation soundings is used in the forward modeling as well as the validation procedure. More details about the 133 GPS/MET occultations can be found in Zou *et al.*, [2002].

## 2.2 Removing the large mismatch in the simulated impact parameter

In one of our early works [Liu *et al.*, 2001], an impact parameter offset correction was found necessary to remove a large mismatch in the simulated impact parameter by the 2D model compared with the GPS/MET data. The impact parameter offset in that study was defined as:

$$\Delta a = a_t^{40 \text{ km}} - a_{GPS}^{40 \text{ km}} \quad (6)$$

where  $a_t^{40 \text{ km}}$  and  $a_{GPS}^{40 \text{ km}}$  were the simulated and the observed GPS/MET impact parameters, respectively, at an altitude of 40 km at the perigee point. For the 837 GPS/MET soundings assimilated in [Liu *et al.*, 2001], the average mean value of  $\Delta a$  was as large as 526 m and the standard deviation was 299 m.

Causes for this impact parameter offset to happen were not explored in Liu *et al.* [2001]. In this study, we find out that such a large difference in the impact parameter is caused by the inconsistency between the ambiguous definitions of the “occultation point” used in the forward model and the GPS/MET data for the calculation of the radius of the Earth’s local curvature. In the original 2D forward model, the vertically averaged perigee location of the observed occultation profile was used to determine the “occultation point” and then the radius of the local curvature center. In the GPS/MET data, however, the perigee point location of the lowest ray of the profile was used. The vertically averaged perigee location of an occultation profile generally differs significantly from the perigee point location of the lowest ray of the profile. Three typical profiles are shown in Fig. 1. It can be seen that the latitude of the perigee point can vary by as much as 0.9 degrees relative to its lowest position at a height of 50 km. The inconsistency in the definitions of the “occultation point” will

cause significant error in the calculation of the radius of the Earth’s local curvature center (about 1 km per degree latitude).

Such an error in the radius of the Earth’s local curvature center will result in an error in the derived impact parameter. In the 2D ray-tracing model and the GPS/MET data, the Earth is assumed spherical with a single radius ( $r_{loc}$ ) of local curvature for all the rays of each occultation. At the tangent point,  $r_{loc}$  is related to the impact parameter at the tangent point through the following relationship:

$$a_t = n * (z + r_{loc}) \quad (7)$$

where  $n$  is the index of refraction and  $z$  is the tangent point height. Therefore, a modification is made to the 2D forward ray-tracing model, which also uses the perigee point location of the lowest ray of the profiles for determining the “occultation point” and the radius of the Earth’s local curvature center. The impact parameter offset with and without this modification for the 133 soundings are shown in Fig. 2. Without correcting the “occultation point” for the calculation of the earth local curvature center, the maximum of the mismatch is as high as 700 meters. The mismatch between the simulated and observed impact parameter at 40 km is significantly reduced for each of 133 soundings. The RMS value of the difference between the simulation and observations is 200 m without the correction. This value decreases to 20 m with the correction.

### 2.3 Changing the starting point scheme for ray integration

As seen in Section 2.1, one major simplification made in the original 2D forward model was the determination of the initial position and the initial direction of a ray at the initiation of the ray integration. This simplification, however, introduces errors in the simulation of the

true ray path and the associated impact parameter and bending angle, especially in the lower troposphere, where the bending angle of the ray is larger. Figure 3 illustrates what could happen for a simulated ray path with the original starting point scheme. Due to the large ray bending near the perigee point, the virtual GPS position determined in the original model will not be close to the true GPS position. The simulated ray paths starting from the virtual GPS position will go through an atmosphere below the observed perigee point height and the tangent direction of the simulated ray path at the perigee point will also not be parallel to the observed ray tangent direction. One obvious consequence of such a simplification in the determination of the initial conditions for the ray integration is an expected negative bias in the impact parameter calculation. This is verified in the calculated bias of the impact parameter at the LEO satellite location, as shown in Fig. 4a. It can be seen that the bias in the simulated impact parameter is negative and it can be as large as -1.4 km in the lower troposphere and -500 m at an altitude of 10 km. The RMS error of the simulated impact parameter have similar magnitudes (Fig. 4b).

Since most ray bending occurs near the perigee point [Melbourne *et al.*, 1994], the simulated ray path should be kept close to the ray's position and direction estimated from observational data at the perigee point. Therefore, a new starting point scheme for the ray integration [Kuo *et al.*, 2000] is introduced into the 2D model. In the new starting point scheme, the ray integration starts from the observed perigee point of each ray and the ray integration is carried out in two opposite directions, one toward the LEO satellite and the other toward the GPS satellite. This will ensure that the impact parameter and the tangent direction of the simulated rays at the perigee point location are very close to the observed impact parameter and tangent direction. Specifically, the new scheme works in the following manner:

1. Starting from the tangent point,  $\vec{x}_p$ , the ray equation is integrated toward the LEO satellite with the observed tangent direction at the perigee point ( $\vec{u}_p^t$ ) used as the initial tangent direction  $\vec{y}_0$ . The ray integration stops at a position where its distance to the earth's surface is 730 km. This position is taken as the LEO satellite position.
2. Starting from the same tangent point,  $\vec{x}_p$ , the ray equation is integrated toward the GPS satellite with  $-\vec{u}_p^t$  as the initial tangent direction  $\vec{y}_0$ . The ray integration stops at a location where its distance to the earth's surface is 20,200km. This location is taken as the GPS satellite position.

The bias and RMS differences of the simulated impact parameter with the new starting point scheme are shown in Fig. 5. It can be seen that with the new starting point scheme, the bias and RMS error are significantly reduced (comparing Fig. 5 with Fig. 4). The negative bias, which can be as large as -1.4 km in the original scheme, is reduced to only 10 m throughout the entire atmosphere. The RMS error is also significantly reduced.

Improvements can also be found in the simulated bending angle. Figs. 6 and 7 show the simulated bending angles before being interpolated to observed impact parameter for the original starting point scheme and the new starting point scheme, respectively. It can be seen that the fractional bias and RMS error can be as large as 35% in the lower troposphere with the original starting point scheme (Fig. 6). With the new starting point scheme, however, the bias is reduced to less than 0.07% and RMS error to less than 0.15% in the lower troposphere (Fig. 7).

Historically, to reduce the impacts of the large simulation errors, the bending angle as a function of the impact parameter, not of individual rays, has been assimilated into the global analysis [Zou *et al.*, 1999]. This has been done through an interpolation of the simulated

bending angle profile, as a function of the simulated impact parameter, to the observed impact parameter. Such a procedure can avoid a large portion of the error in the simulated bending angle introduced by a large error in the simulated impact parameter, as was the case with the original starting point scheme. This argument is supported by the numerical results shown in Fig. 8a. Although the bias and RMS error with and without the new starting point scheme are significantly different, with two orders of magnitude difference for the simulated bending angles (Figs. 6 and 7), the difference in the errors after the interpolation becomes much smaller.

However, the bias and RMS error after the interpolation with the original start point scheme in Fig. 8 remain quite large in the lower troposphere. The new starting point scheme is able to further reduce these errors (see dashed lines in Fig. 8), by more than 50%.

## 2.4 Deriving the bending angle using Snell's law

Another major difference between the original 2D ray-tracing model and the GPS/MET data was the derivation of the bending angle. As described in section 2.1, the bending angle was calculated as the angle between the two tangent directions of the ray at the GPS and LEO satellite locations in the 2D model. It is also worth mentioning that the impact parameter at the GPS location is not necessarily the same as the impact parameter at the LEO position in the 2D model simulation. However, the bending angle in the GPS/MET data was derived from the Doppler frequency shift under the application of Snell's law, that is, the impact parameters at the LEO and GPS satellite locations were assumed equal. Snell's law has to be applied because the true refractivity and its gradient are not known. This inconsistency between the observations and the forward model could introduce errors to the forward modeling of the GPS/MET bending angle observation when the difference

between the impact parameters at the LEO and GPS satellites is large. In order to be consistent with the derivation of the GPS/MET bending angle observation, the derivation of the bending angle using Snell's law is now incorporated into the 2D model. The main idea of the procedure follows what was described in Appendix A of Zou *et al.* [1999] for deriving GPS/MET bending angle observations, with a few variations (Step 1 and 2 below). Details of the procedure are as follows:

**Step 1:** Integrate the ray equation from the perigee point ( $\vec{x}_p$ ) to the GPS and LEO positions ( $\vec{x}_G$  and  $\vec{x}_L$ ), and obtain the ray tangent directions at the GPS and LEO positions ( $\vec{u}_G^t$  and  $\vec{u}_L^t$ ).

**Step 2:** Calculate the Doppler shift ( $f_d$ ) for the simulated rays according to the ray positions ( $\vec{x}_G$  and  $\vec{x}_L$ ) and the ray directions ( $\vec{u}_G^t$  and  $\vec{u}_L^t$ ) using the observed velocities of the GPS and LEO satellites,  $\vec{v}_G$  and  $\vec{v}_L$ , approximately:

$$f_d = f_c \left( \frac{c - n_L \vec{v}_L \cdot \vec{u}_L^t}{c - n_G \vec{v}_G \cdot \vec{u}_G^t} - 1 \right) \quad (8)$$

where  $n_G$  and  $n_L$  are the refractivity index at the GPS and LEO satellite locations.

Introducing  $\phi_G$  and  $\phi_L$  to represent the angles between the satellite radii ( $\vec{r}_G$  and  $\vec{r}_L$ ) and the tangent direction vectors ( $\vec{u}_G^t$  and  $\vec{u}_L^t$ ), the Doppler shift (Eq. 8) can be written as:

$$f_d = f_c \left( \frac{c - n_L (v_L^r \cos \phi_L - v_L^t \sin \phi_L)}{c - n_G (v_G^r \cos \phi_G - v_G^t \sin \phi_G)} - 1 \right) \quad (9)$$

where  $v_G^r$  and  $v_G^t$  are the radial and tangent components, respectively, of the GPS satellite velocity in the ray plane, and  $v_L^r$  and  $v_L^t$  are for the LEO velocity components.

The Doppler shift corresponding to the straight line signal path connecting the GPS and LEO satellite is:

$$f_0 = f_c \left( \frac{c - n_L \vec{v}_L \cdot \vec{u}_s}{c - n_G \vec{v}_G \cdot \vec{u}_s} - 1 \right) \quad (10)$$

where  $\vec{u}_s$  is the unit vector pointing from the GPS satellite to the LEO satellite and  $c$  is the speed of light in a vacuum.

Additionally, the Doppler shift due to the bending of rays can be obtained as:

$$\Delta f = f_d - f_0 \quad (11)$$

**Step 3:** Calculate the two satellite zenith angles ( $\phi_G$  and  $\phi_L$ ) by solving the following two equations:

$$\Delta f = f_c \left( \frac{c - n_L (v_L^r \cos \phi_L - v_L^t \sin \phi_L)}{c - n_G (v_G^r \cos \phi_G - v_G^t \sin \phi_G)} - 1 \right) - f_0 \quad (12)$$

$$a = r_G n_G \sin \phi_G = r_L n_L \sin \phi_L \quad (\text{Snell's law}) \quad (13)$$

**Step 4:** Finally, obtain the impact parameter at the LEO position and the bending angle of the ray:

$$\begin{aligned} a &= r_L n_L \sin \phi_L \\ \alpha &= \phi_G + \phi_L + \arccos \left( \frac{\vec{r}_G \cdot \vec{r}_L}{r_G r_L} \right) - \pi \end{aligned} \quad (14)$$

Numerical results from the 133 GPS/MET occultations show that the derived impact parameter and bending angle with the application of Snell's law are not significantly different from those obtained in the original model at the T126L28 resolution (figures omitted). This is probably due to the fact that the refractivity fields at the T126L28 resolution may not contain strong enough horizontal inhomogeneous variations. Figure 9 shows the RMS difference between the simulated impact parameters at the LEO and GPS locations. It is

found that the difference is only about 27 meters in the lower troposphere, which is quite small. Therefore, the violation to the spherical symmetry assumption implied in Snell's law is not large enough to make a significant difference in the simulated bending angle. Further test on the necessity of incorporating the derivation of the bending angle using Snell's law is still required if an analysis of higher resolution is used.

## 2.5 Reducing the computational cost of the ray-tracing model

In the original 2D ray-tracing model, a constant step size was used for the ray integration when the ray path is within the atmosphere, that is, when the distance of the ray path to the Earth's surface is less than 100 km. In order to reduce the computational cost of the 2D model, an effort is made here to test the feasibility of a variable step size for the ray integration within the atmosphere. It is known that in the upper atmosphere, the atmospheric refractivity and its variations are much smaller compared with the lower atmosphere. Therefore, a larger step size may be used for the ray integration in the upper atmosphere to increase the computing efficiency, with minimal impacts on the accuracy of the ray integration.

A preliminary scheme of the variable step size is proposed for the 2D model as follows:

$$\Delta\tau = \begin{cases} \Delta\tau_{ori}; & r_0 < r_c \\ 2\Delta\tau_{ori} & r_0 \geq r_c \end{cases} \quad (15)$$

where  $r_0$  is the distance of the ray to the Earth's surface,  $\Delta\tau_{ori}$  is the step size in the original model (2 km), and  $r_c$  is an adjustable prescribed constant parameter (between 100 km, the approximate depth of the atmosphere, and 0 km). In other words, the scheme sets two step sizes above and below a prescribed constant height value  $r_c$  before the ray integration starts.

This avoids the nonlinearity which could be introduced by adaptive step sizes based on data type [Healy, 2002]. In the later case, the linearization of the raytracing operator would involve the derivative of the step size scheme which would render the forward raytracing problem more nonlinear and the backward raytracing procedure more complicated.

A few values of  $r_c$  are tested. The case where  $r_c = 60$  km turns out to be a reasonable choice. The difference of the bias and RMS error of the bending angle (after interpolation to the observed impact parameter) between the single and the variable step size schemes The fractional difference of the bias and RMS error are about three orders of magnitude smaller than the differences introduced by changing the starting point scheme (compare with Fig. 8). Therefore, the impacts of increasing the step size on the accuracy of the simulated bending angle profile is negligible. The CPU time for the forward modeling of the 133 GPS/MET soundings and 10 Hz resolution using the variable step size scheme is now only 1700 seconds on a CRAY J90, compared with 2200 seconds for the single step size case of the original model. That is, the CPU time for the new scheme is now only 77% of the original scheme.

### 3 Impacts on bending angle assimilation

#### 3.1 Experiment design

To further examine the impacts of the modifications to the 2D forward ray-tracing model discussed in the previous section, two data assimilation experiments are carried out with and without these modifications. Since the incorporation of Snell's law in the derivation of the bending angle does not contribute significantly to the improvement of the bending angle simulation at T126L28 resolution, this modification is not included in these experiments.

The NCEP SSI analysis system at T62L28 resolution [*Parrish and Derber, 1992; Derber and Wu, 1998*] is used in these experiments. This system produces an optimal analysis of wind, temperature, moisture, and surface pressure through a minimization of an objective function, which consists of three terms: a weighted square of background increments, a weighted square of the observational increments, and a weighted square of the small divergence time tendency. Details on the incorporation of the GPS/MET data into the NCEP SSI system can be found in *Zou et al. [2000]*.

In this study, the GPS bending angle “observation” and other GPS inputs (such as tangent directions at the perigee points) required for the 2D ray-tracing model are derived from the accurate 3D ray-tracing model based on the refractivity calculated from the NCEP T126L28 high resolution analysis, as described in section 2.1. Each of the 133 occultation profiles are assimilated into the data assimilation system, using only GPS bending angle observations for these experiments. For each occultation profile, about 35 rays are assimilated. The vertical interval of these rays is about 0.4 km in troposphere and 2-4 km above the troposphere, which is comparable to the vertical resolution of the NCEP analysis. The weighting for the GPS bending angle observations are taken from *Liu et al. [2001]*, which was defined as the inverse of the mean square difference between the simulated and observed 837 GPS/MET occultation profiles available during June 20-30, 1995.

The background (guess) field is a 6-hour forecast of the NCEP T62L28 model at 12 UTC October 12, 1995. The final optimal solutions of temperature, moisture, and surface pressure obtained with the assimilation of the GPS bending observation will be compared with the “true” temperature, moisture, and surface pressure fields, i.e., the NCEP high resolution (T126L28) analysis at 12 UTC October 12, 1995.

The minimization is carried out in a similar manner to *Zou et al.* [2000]. There are two outer loops (eg, updates for the nonlinear model solution), each of them having 15 inner loops (the total number of iterations for updating the analysis increment within each outer loop). The minimization performs quite well, with a reduction of 5-6 orders of the magnitudes of the norm of the gradient of the cost function and a reduction of 1-2 orders of the magnitudes of the cost function.

### 3.2 Numerical results

The optimal analysis fields of temperature, specific humidity, and surface pressure are interpolated to the 133 GPS/MET occultation locations. The observed profiles of temperature, specific humidity, and surface pressure are obtained by interpolating the NCEP high resolution (T126L28) analysis to the same 133 locations. Since many GPS/MET profiles did not reach lower than 5-7 km, the vertical profiles of the temperature and specific humidity variables are restricted above the same altitude where the bending angle observation is available.

The latitudinal distribution of the lowest altitude reached by each occultation for the 133 soundings is shown in Fig. 11. It can be seen that the GPS/MET occultations in the tropics did not go as low as in the Northern and Southern Hemisphere middle and polar latitudes and there are very few which reached below 2.5 km in the Northern and Southern Hemisphere middle and polar latitudes. Given this large difference in the distributions of the lowest height of these GPS/MET occultations, we have calculated the error statistics in three latitudinal bands: Northern Hemisphere (25N-90N), tropical region (25S-25N) and Southern Hemisphere (25S-90S). Figures 12-14 show the vertical profiles of the bias and RMS error of the specific humidity and temperature in these three latitudinal bands, respectively. It can

be seen that the bias of the specific humidity in the NCEP T62L28 guess field is positive in all three regions, that is, the NCEP T62L28 guess is more moist than the NCEP T126L28 analysis. The GPS bending angle assimilation is able to reduce both the bias and RMS errors significantly. The error in the moisture analysis using the modified ray-tracing model is evidently smaller than that using the original ray-tracing model. Differences in temperature analysis due to the use of modified raytracing scheme in the tropics and Northern Hemisphere is not as significant as for moisture analysis. Improvements in temperature analysis resulting from bending angle assimilation are much more significant in the Southern Hemisphere than in the tropics and Northern Hemisphere.

We point out that in the calculation of the bias and RMS error shown in Fig. 14, the sounding located at (54S, 177W) is excluded for its peculiar behavior. Figure 15 shows the vertical profiles of bending angle errors before and after assimilation (Fig. 15a), as well as the temperature and moisture profiles (Fig. 15b,c) from the truth (T126 NCEP analysis), the guess field, and the two analyses (with and without new modifications). A moisture inversion layer is found in the true profile between 3-4.5 km (solid line in Fig. 15b), which is not captured in the guess field (dashed line in Fig. 15b). Below this inversion layer, the moisture content in the guess field is much higher than the truth. The temperature from the guess field is colder than the truth within the inversion layer (Fig. 15c). The bending angle assimilation, conducted at T62L28 resolution, effectively reduces the differences between modeled and observed bending angles at all vertical levels (Fig. 15a). Such a fit in the bending angle results in an adjustment in the temperature and specific humidity profiles, showing a near perfect specific humidity analysis below the inversion layer and an excellent temperature analysis within the inversion layer (Fig. 15b-c). However, the specific humidity within the inversion layer and the temperature below the inversion layer are slightly degraded.

Noticing that the characteristics of the profile at this sounding location are a local phenomena and can only be captured by the high-resolution model (T126L28), the degradation in temperature and specific humidity analysis near the inversion layer is believed to be caused by the representative error. Features of this sounding (solid lines) from the T126L28 NCEP analysis (the truth) is not resolvable by the coarse resolution (T62L28) model. This may suggest that GPS assimilation with a higher resolution model is needed to better capture observed features in soundings with complicated vertical structures which are very different from their surroundings.

Improving the analysis of surface pressure has been and remains to be a challenge ever since the first GPS/MET data assimilation experiments were conducted [*Zou et al.*, 2000; *Liu et al.*, 2001; *Shao and Zou*, 2002]. It is extremely interesting to examine the impact of these modifications to the 2D ray-tracing model on the surface pressure analysis. The bias and RMS error of the simulated surface pressure for the 133 occultations are shown in Table 1 for the Northern Hemisphere, Southern Hemisphere, and Tropics. In the Northern Hemisphere where the guess field is most reliable and accurate (it can be seen that the bias of the surface pressure guess field is quite small), the bias is slightly increased after the assimilation with the original ray-tracing model. However, the bias of surface pressure in the analysis field is reduced after the assimilation with the modified ray-tracing model. In the Southern Hemisphere (where the bias of the guess field is much larger than the Northern Hemisphere), the bias is slightly increased after the assimilation without the modifications. The degradation in the surface pressure analysis is, however, reduced using the modified ray-tracing model. In the Tropics, the bias of the surface pressure is reduced after the assimilation with both the original and modified ray-tracing model. It should be noted that

the improvement in the surface pressure in the Tropics is most difficult due to that fact that most of the GPS occultations stop at quite a high altitude.

## 4 Conclusions

Data assimilation is concerned with both its efficiency and accuracy. In this paper, several improvements are made to a 2D GPS occultation ray-tracing model. It is found that the original scheme for setting up the initial conditions for the ray integration contributes significantly to the large errors in the simulated ray path and thus in the values of the impact parameter and bending angle. A new starting point scheme is introduced into the 2D ray-tracing model and it greatly improves the accuracy of the model. Snell's law is also incorporated into the derivation of the bending angle of the 2D model which makes the observation operator more consistent with the GPS/MET bending angle observations. It is also found that the large impact parameter offset in the original 2D model is mainly caused by the inappropriate or ambiguous determination of the "occultation point". In addition, a variable step size for the ray integration is tested, which significantly reduces the computational cost while maintaining a similar level of accuracy compared to the more expensive constant step size scheme.

The data assimilation experiments incorporating a total of 133 bending angle profiles from the GPS/MET experiments with and without these modifications indicate that the modifications improve the analysis accuracy of not only the specific humidity and temperature fields, but also the surface pressure field. The most significant improvements are observed in the lower troposphere.

We realize that results presented in this paper are limited to model-generated data and a limited number of occultations. Further testing of the modified ray-tracing model will be followed. Future plans include further testing of the improved forward ray-tracing model at a higher resolution while assimilating new GPS observations, such as those from CHAMP and SAC-C experiments. The observations from these experiments are expected to have much better quality in the lower troposphere and to penetrate more deeply into the lower troposphere as a result of better hardware and firmware. It is expected that the improved 2D ray-tracing model will also reduce the forward modeling error and therefore benefit the assimilation of these GPS data in the lower troposphere. In addition, a higher resolution (T170L42) paralleled GPS data assimilation system, which was recently developed on IBM SP parallel supercomputers, will be used to test the necessity of incorporating Snell's law into the derivation of the bending angle in the ray-tracing model at these higher resolutions.

#### *Acknowledgments*

This research is supported by the Integrated Program Office of NOAA National Polar-orbiting Operational Environmental Satellite System under SMC/CIPN Project Order No. Q000C1737600086. The authors would like to thank Dr. S. Lord for his continuing support to the GPS data assimilation work. The authors would also like to thank Dr. S. Sokolovskiy for his very helpful suggestions on improving the forward ray-tracing model.

## **5 References**

- Derber, J.C., and W.S. Wu, The use of TOVS cloud-cleared radiances in the NCEP's SSI analysis system, *Mon. Wea. Rev.*, *126*, 2287-2299, 1998.
- Hoeg, P., A. Hauchecorne, G. Kirchengast, S. Syndergaard, B. Belloul, R. Leitinger, and W. Rothleitner, *Derivation of the atmospheric properties using radio occultation technique*, Danish Meteorological Institute, Scientific Rep. 95-4, 208pp, 1995.
- Kuo Y. H., S. Sokolovsky, R. A. Anthes, and F. Vanderberghe, Assimilation of GPS Radio occultation data for numerical weather prediction, *TAO*, *11*, 157-186, 2000.
- Kursinski, E.R. et al., Initial results of radio occultation observations of Earth's atmosphere using GPS, *Science*, *271*, 1107-1110, 1996.
- Liu H., Zou X., H. Shao, R. Anthes, J. Chang, J. Tseng, and B. Wang, Impact of 837 GPS/MET bending angle profiles on assimilation and forecasts for the period June 20-30, 1995, *J. Geophys. Res.*, *106*, 31771-31786, 2001.
- Matsumura, T., J. Derber, and J. Yoe, F. Vandenberghe, and X. Zou, The inclusion of GPS limb sounding data into NCEP's global data assimilation system. *NWS Office Note 426*, NOAA/NCEP/NWS, 26pp, 1999.
- Melbourne, W. G., E. S. Davis, C. B. Duncan, G. A. Hardy, E. R. Kursinski, T. K. Meehan, L. E. Young, and T. P. Yunck, *The Application of Space-borne GPS to Atmospheric Limb Sounding and Global Change Monitoring*, JPL Publication 94-18, National Aeronautics and Space Administration and Jet Propulsion Laboratory, California Institute of Technology, Pasadena, California. pp147, 1994.
- Palmer, P. I., J. J. Barnett, J. E. Eyre, and S. B. Healy, Application of an optimal estimation inverse method to GPS/MET bending angle observations, *J. Geophys. Res.*, *106*, 17,147-17,160, 2001.

- Parrish, D.F., and J. Derber, The National Meteorological Center's spectral and statistical-interpolation analysis system, *Mon. Wea. Rev.*, *120*, 1747-1763, 1992.
- Rocken, C., R. Anthes, M. Exner, D. Hunt, S. Sokolovskiy, R. Ware, M. Gorbunov, W. Schreiner, D. Feng, B. Herman, Y.-H. Kuo, and X. Zou, Analysis and validation of GPS/MET data in the neutral atmosphere. *J. Geophys. Res.*, *102*, 29,849-29,866, 1997.
- Shao, H. and X. Zou, The impact of observational weighting on the assimilation of GPS/MET bending angle, *J. Geophys. Res.*, (accepted), 2002.
- Syndergaard, S., Modeling the impact of the earth's oblateness on the retrieval of temperature and pressure profiles from limb sounding. *J. Atmos. Solar-Terr. Phys.*, *60*, 171-180, 1998.
- Ware R., et al., GPS sounding of the atmosphere from low earth orbit: Preliminary results, *Bull. Am. Meteorol. Soc.*, *77* 19-40, 1996.
- Zou, X. F. Vandenberghe, B. Wang, M. Gorbunov, Y. Kuo, et al.: A ray-tracing operator and its adjoint for the use of GPS/MET refractivity angle measurements, *J. Geophys. Res.*, *104*, 22301-22318, 1999.
- Zou X., B. Wang, H. Liu, R.A. Anthes, T. Matsumura, and Y.-J. Zhu, Use of GPS/MET refraction angles in 3D variational analysis, *Quart. J. Royal Meteorological Society*, *126*, 3013-3040, 2000.
- Zou X., Hui Liu, and R.A. Anthes: A statistical estimate of errors in the calculation of radio-occultation bending angle caused by a 2D approximation of ray tracing and the assumption of spherical symmetry of the atmosphere, *Journal of Atmospheric and Oceanic Technology*, *19*, 51-64, 2002.

## Figure Captions

Figure 1: The latitudinal shifts of the perigee points relative to its lowest perigee point position for 3 random selected occultation profiles of the 133 GPS/MET soundings.

Figure 2: The impact parameter offset for the 133 GPS/MET occultation profiles available on October 11, 1995 with (shaded bars) and without (clear bars) the modification to the calculation of the “occultation point”.

Figure 3: A schematic illustration of simulated ray paths with the original and new starting point schemes.

Figure 4: (a) The bias and (b) RMS error of the simulated impact parameter with the old starting point scheme.

Figure 5: Same as Fig. 4 except with the new starting point scheme.

Figure 6: (a) The bias and (b) RMS error of the simulated bending angle with the old starting point scheme.

Figure 7: Same as Fig. 6 except with the new starting point scheme.

Figure 8: Same as Figs. 6 and 7 except that the simulated bending angle, as a function of the simulated impact parameter, is interpolated to the observed impact parameter. Solid line: the original starting point scheme. Dashed line: the new starting point scheme.

Figure 9: The RMS difference between the simulated impact parameter at the LEO and GPS location of each ray for the 133 GPS/MET occultations at T126L28 resolution (unit: m).

Figure 10: The (a) bias and (b) RMS error between the variable step size scheme and the single step size scheme.

Figure 11: The lowest heights reached by the 133 GPS/MET occultation profiles with respect to latitude.

Figure 12: The bias (left panels) and RMS error (right panels) of the moisture (upper panels) and temperature (lower panels) analysis in the Northern Hemisphere (25N - 90N). The solid line represents the error in guess field, dashed line for the original ray-tracing model, and dotted line for the modified model.

Fig. 13: Same as Fig. 12 except for the tropical region (25N - 25S).

Fig. 14: Same as Fig. 12 except for the Southern Hemisphere (25S - 90S).

Fig. 15: Vertical profiles of (a)  $\alpha - \alpha^{obs}$  before (solid line) and after (dashed line using original scheme, dotted line using modified scheme) assimilation, (b) specific humidity and (c) temperature from the truth (thick solid line), the guess field (thin solid line), and the two analyses after bending angle data assimilation (dashed line using the original scheme, dotted line using the modified scheme).

Table 1: The bias and RMS error in the simulated surface pressure (unit: hPa).

	guess field	analysis without modifications	analysis with modifications
	<b>Northern Hemisphere</b>		
bias	0.7	0.9	0.6
RMS error	7.1	7.1	7.1
	<b>Southern Hemisphere</b>		
bias	4.5	4.8	4.7
RMS error	11.5	11.5	11.5
	<b>Tropics</b>		
bias	2.7	2.5	2.6
RMS error	5.8	5.9	5.9

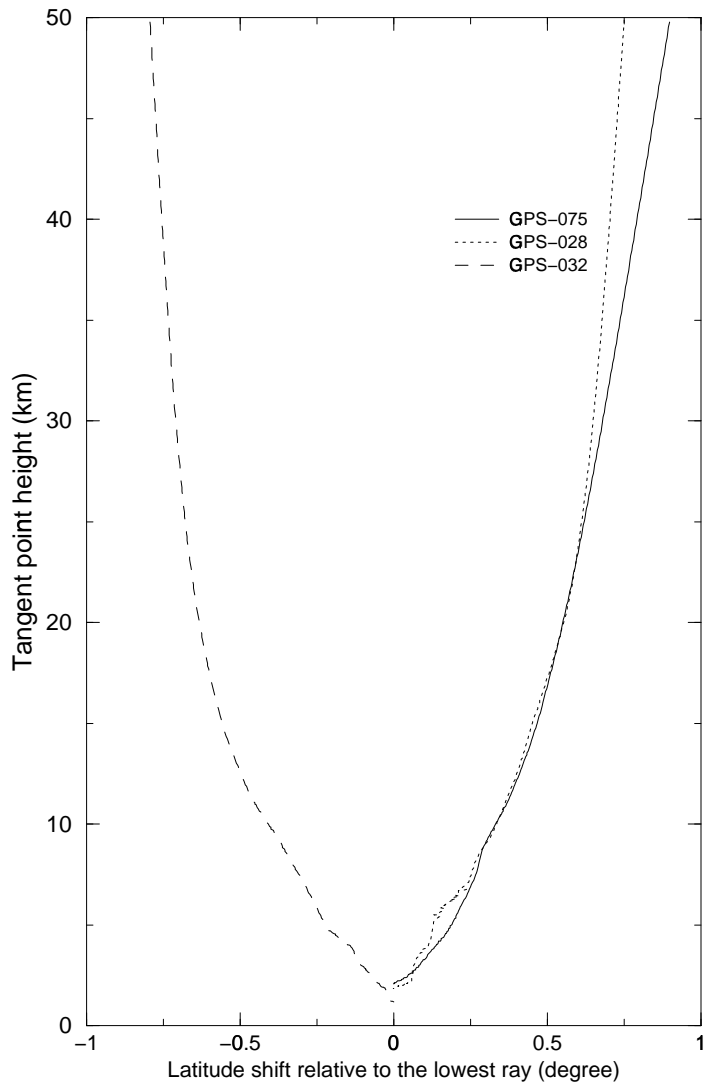


Fig. 1

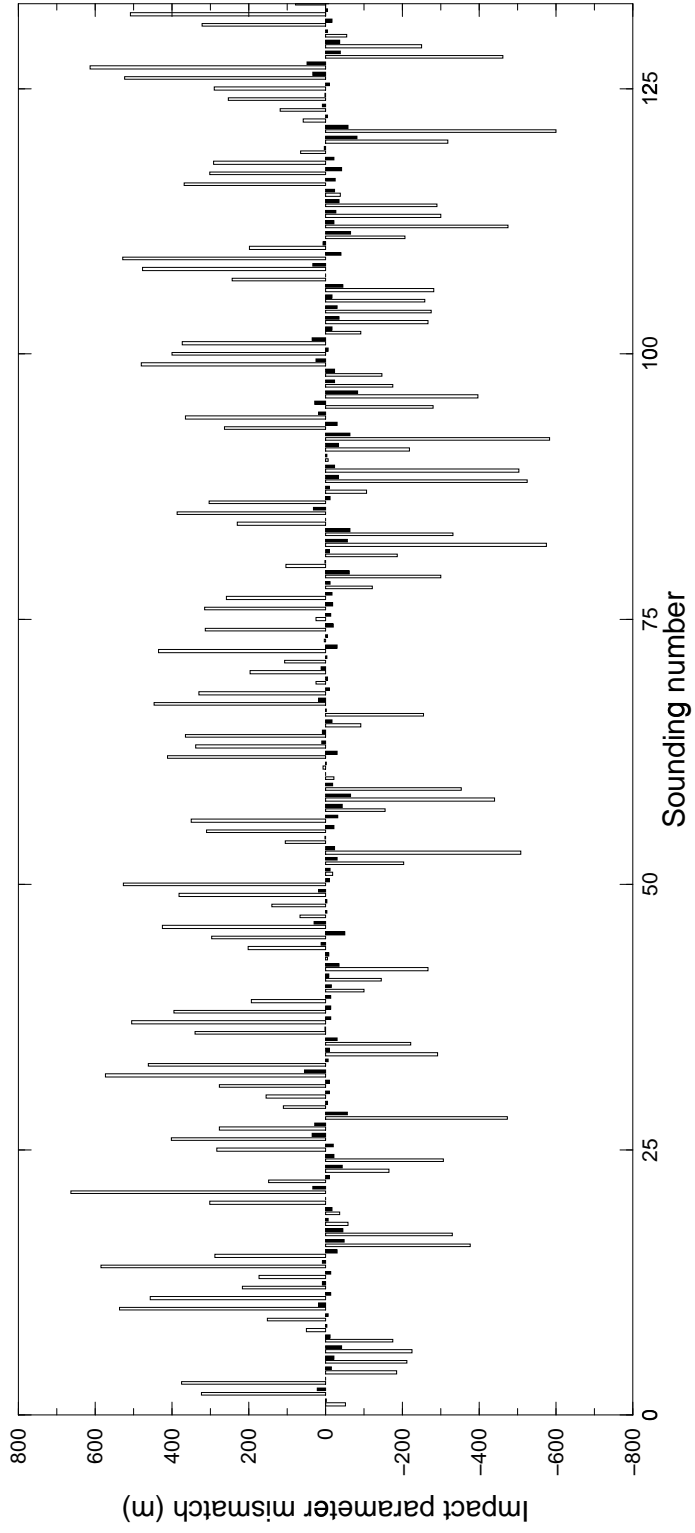


Fig. 2

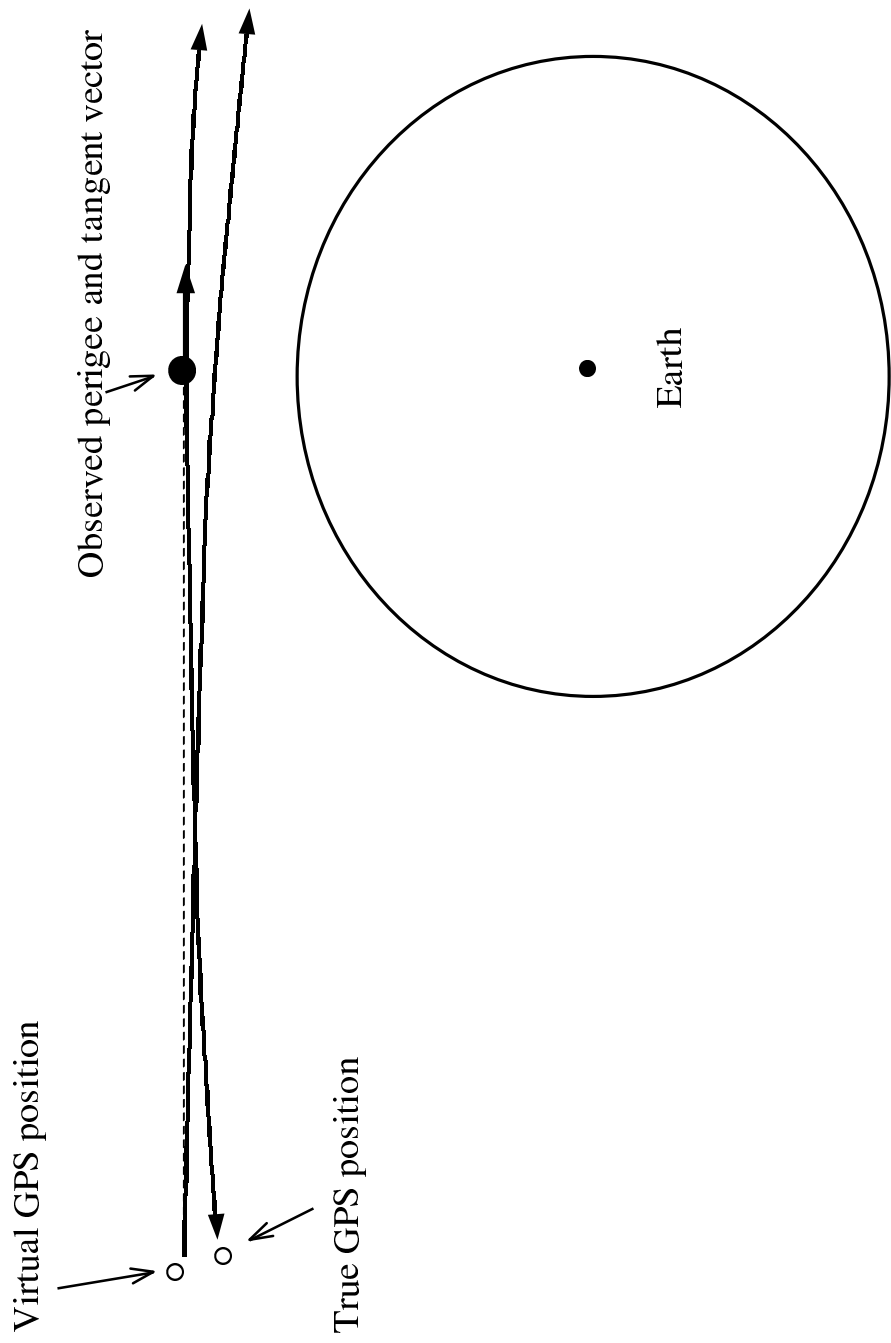


Fig. 3

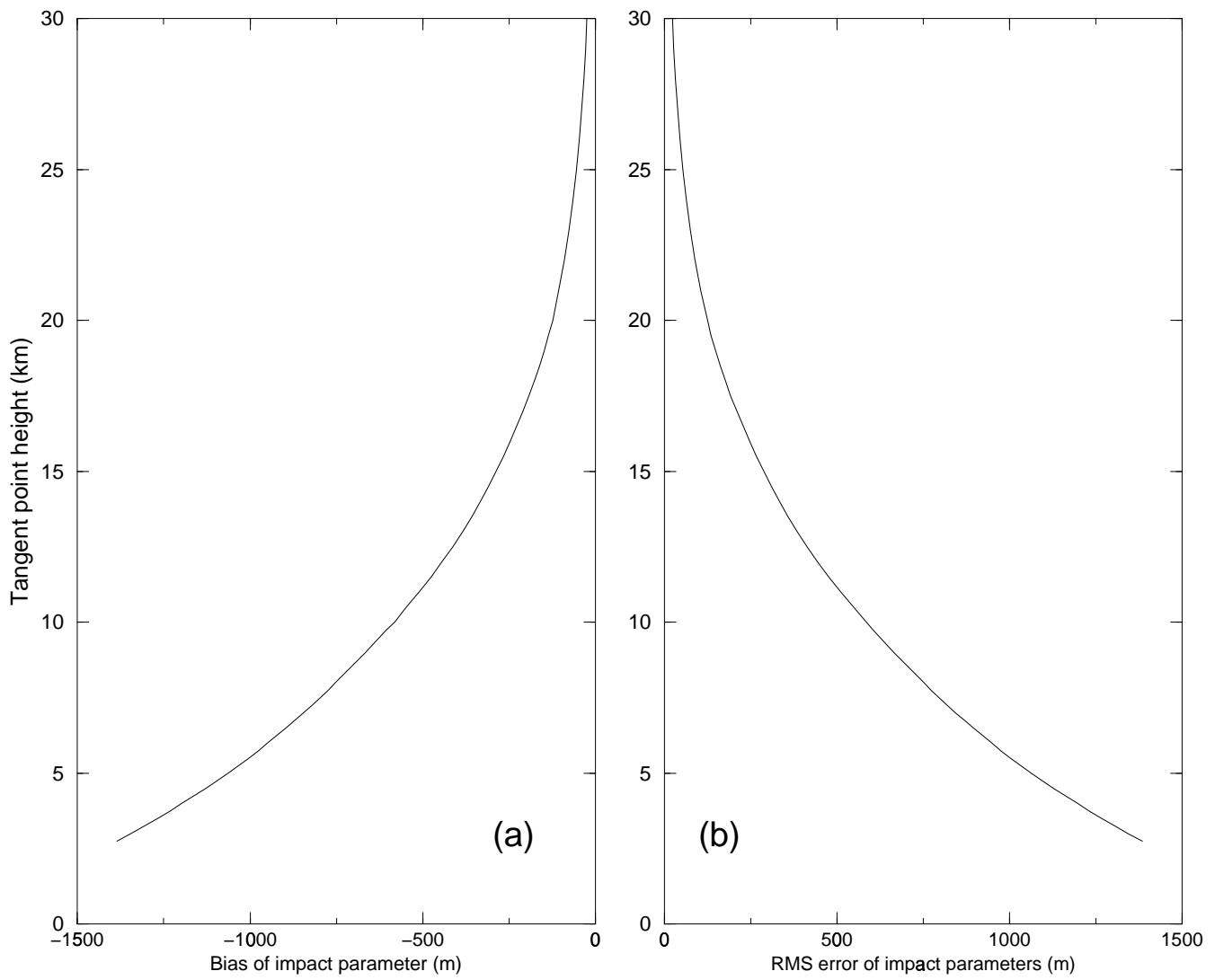


Fig. 4

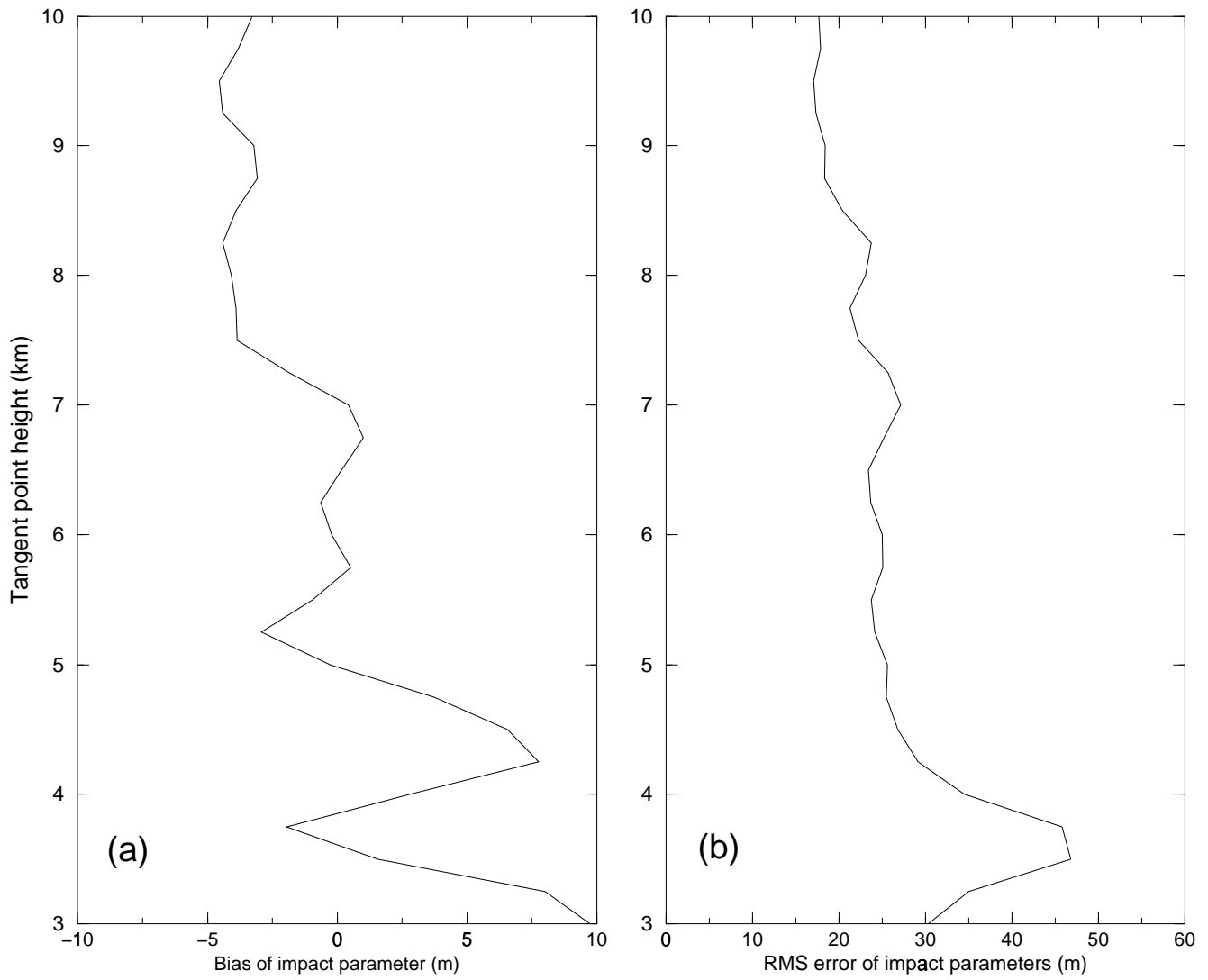


Fig. 5

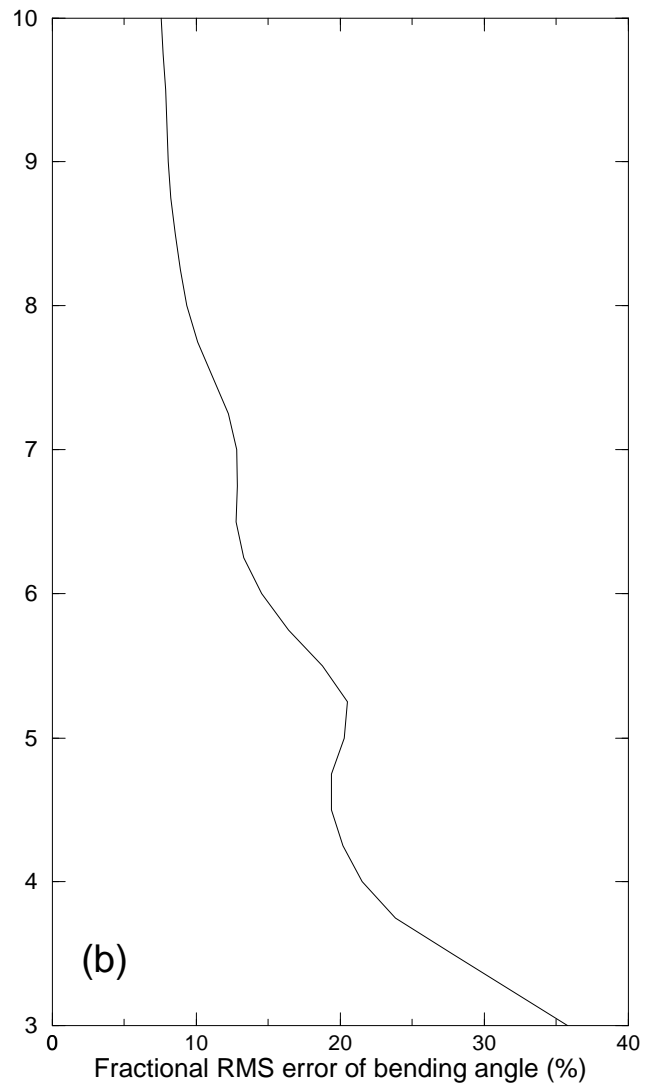
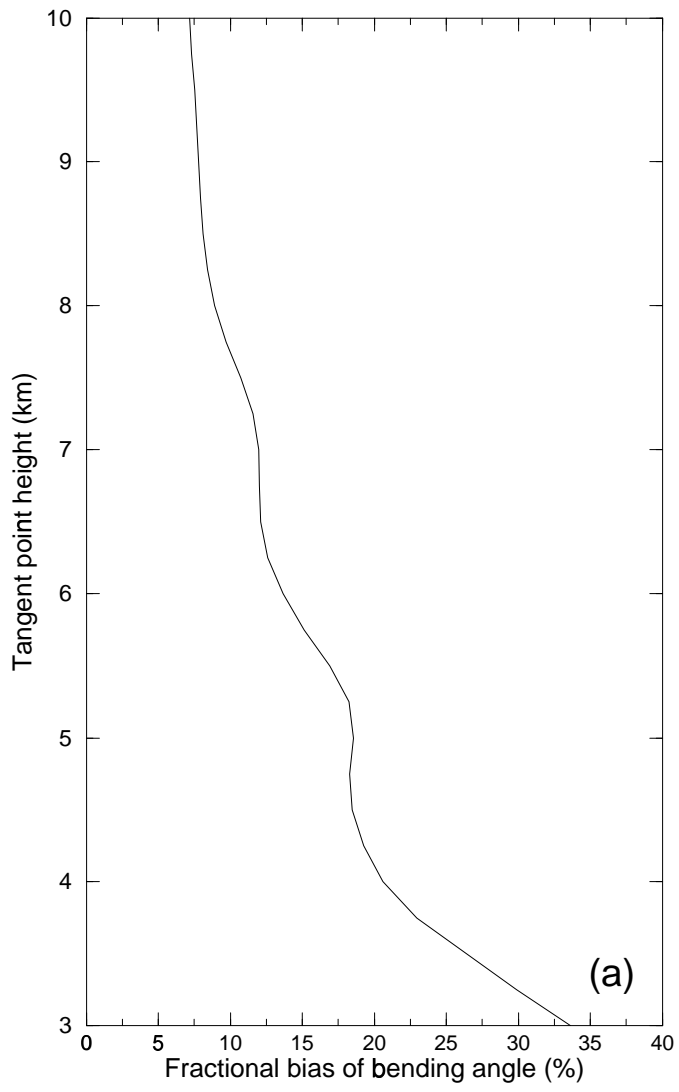


Fig. 6

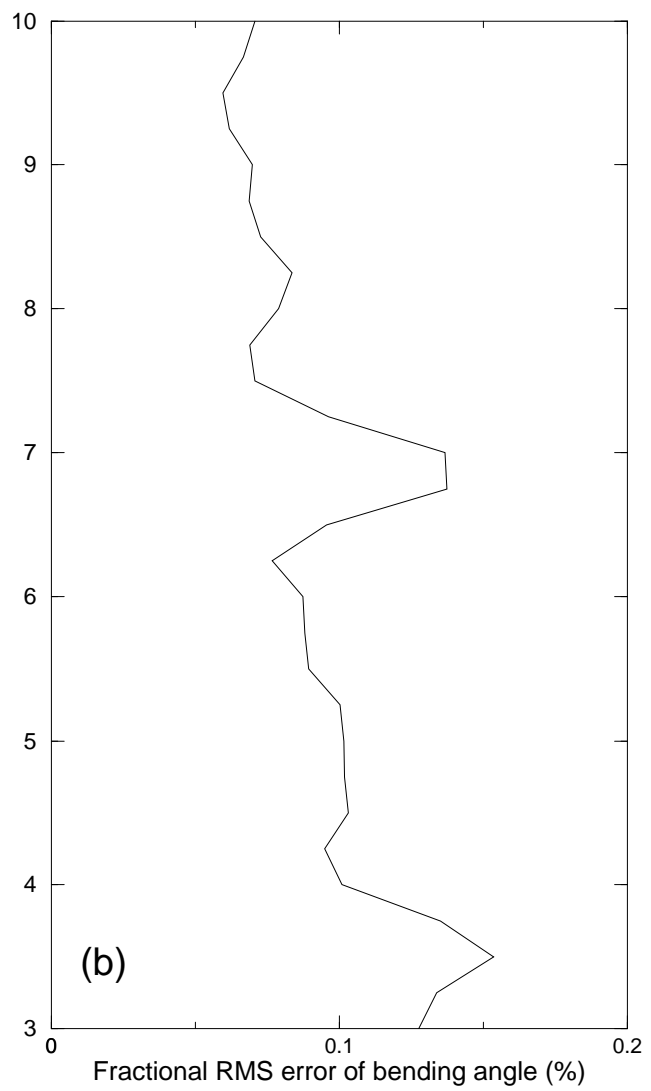
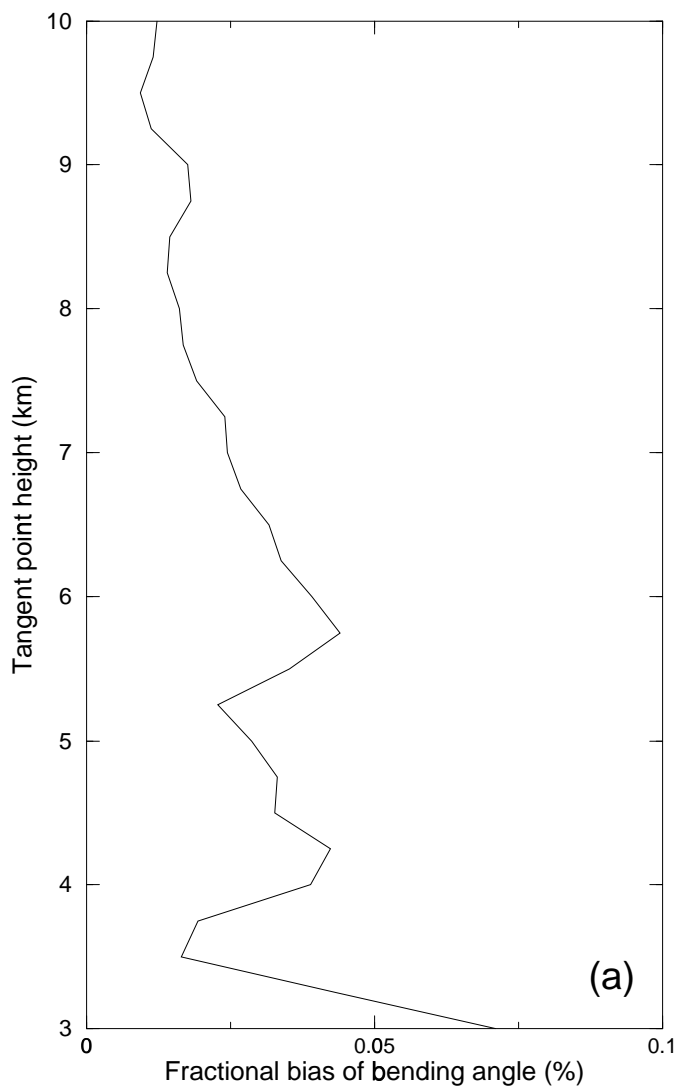


Fig. 7

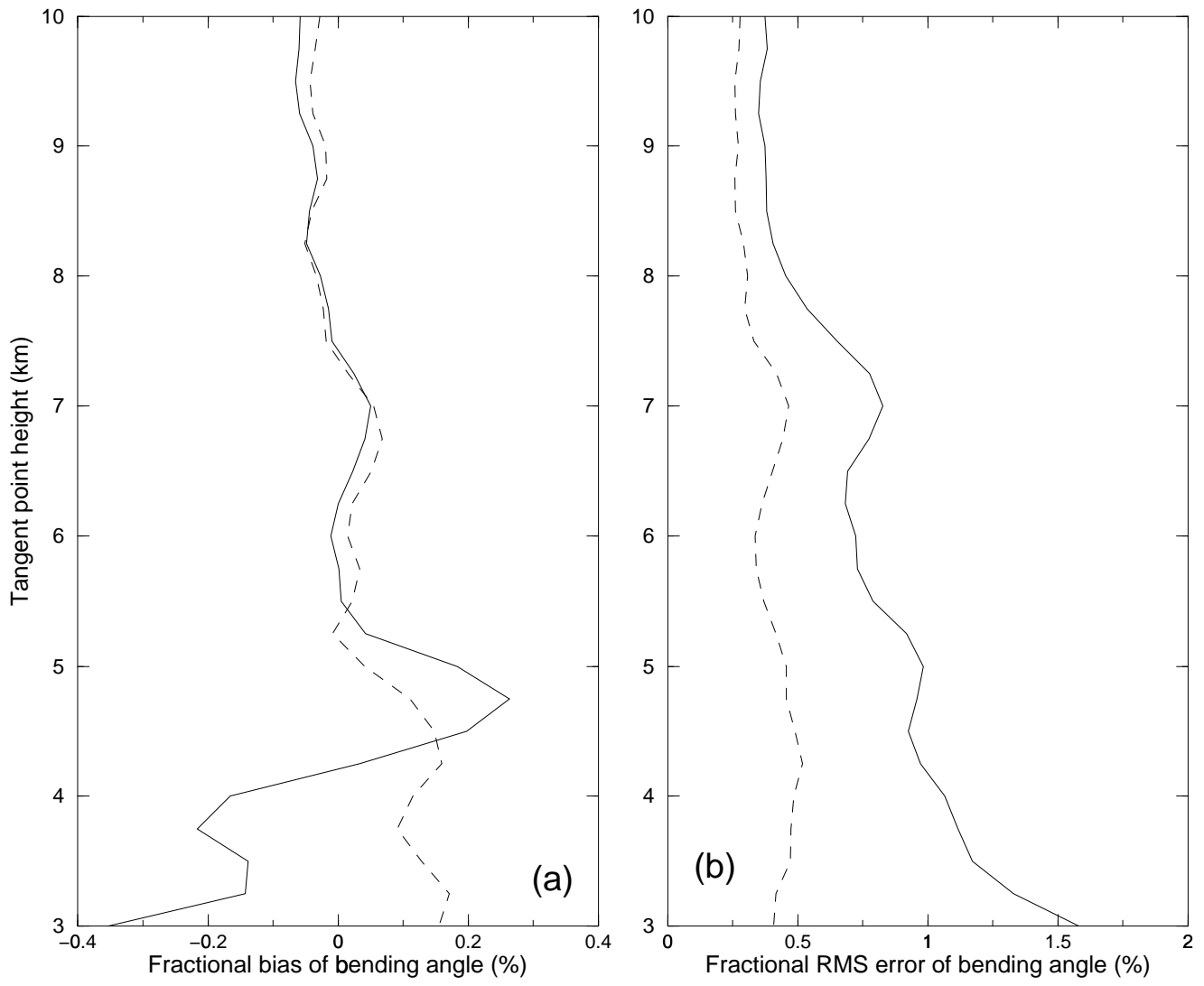


Fig. 8

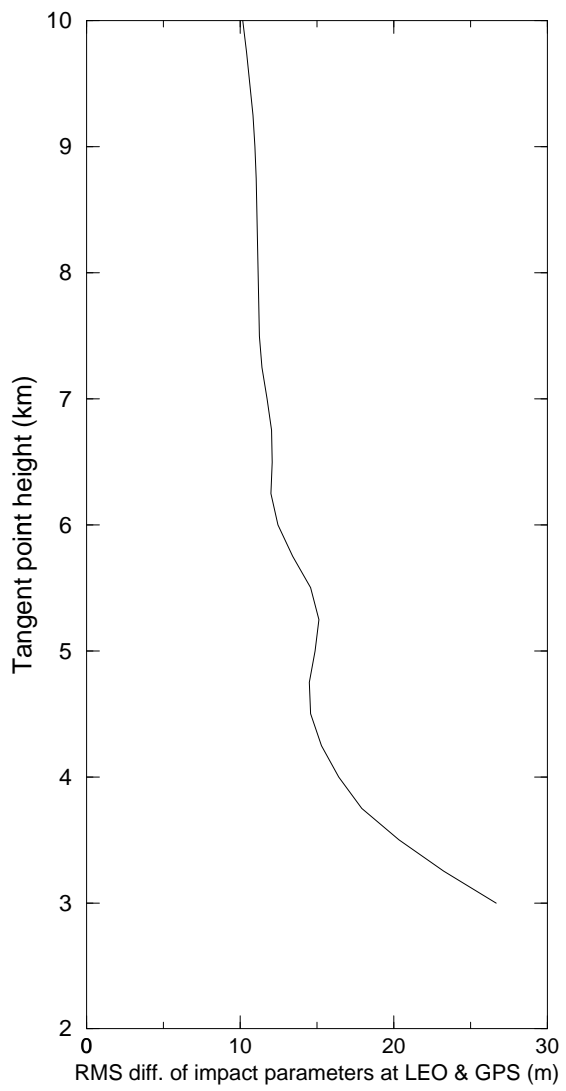


Fig. 9

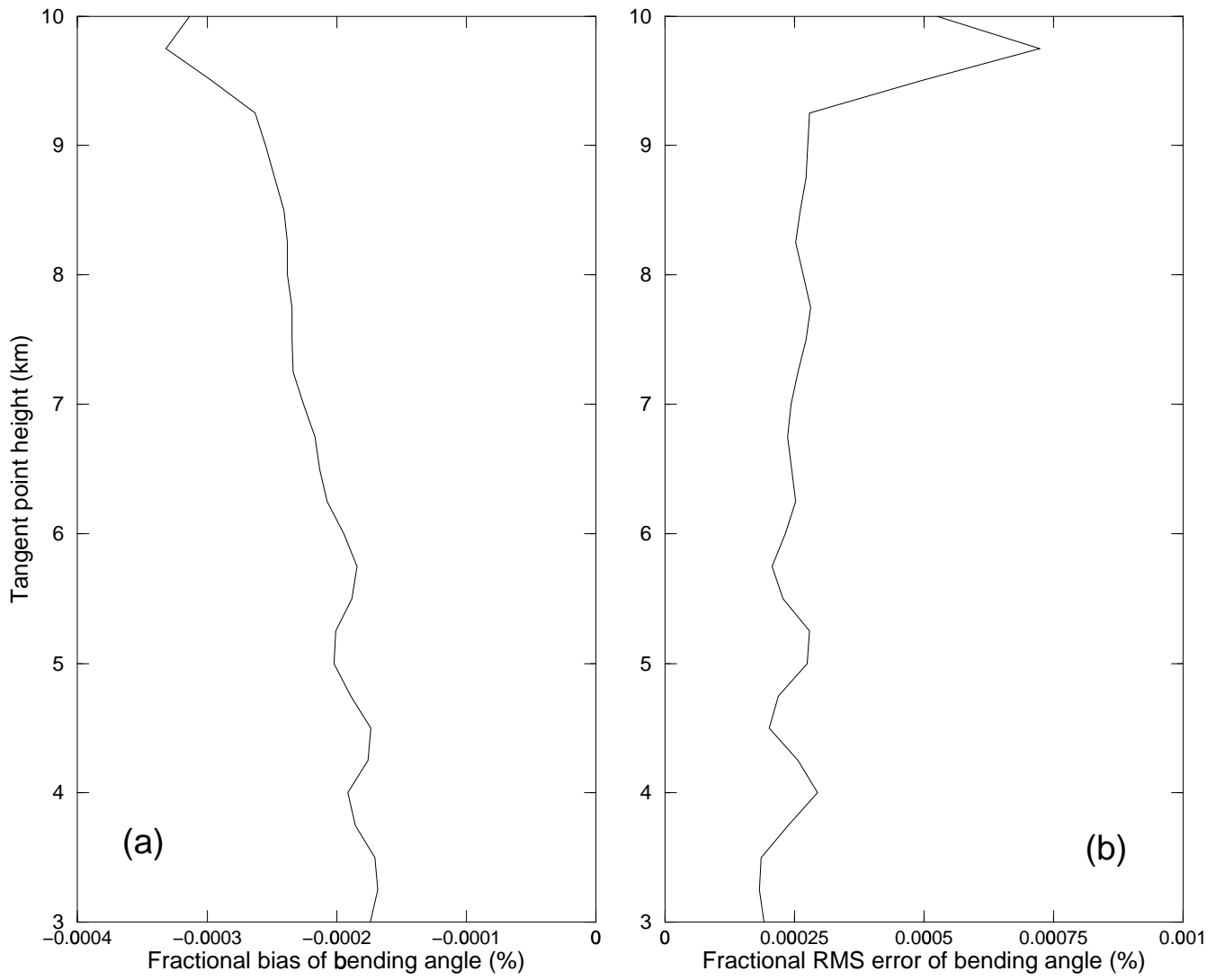


Fig. 10

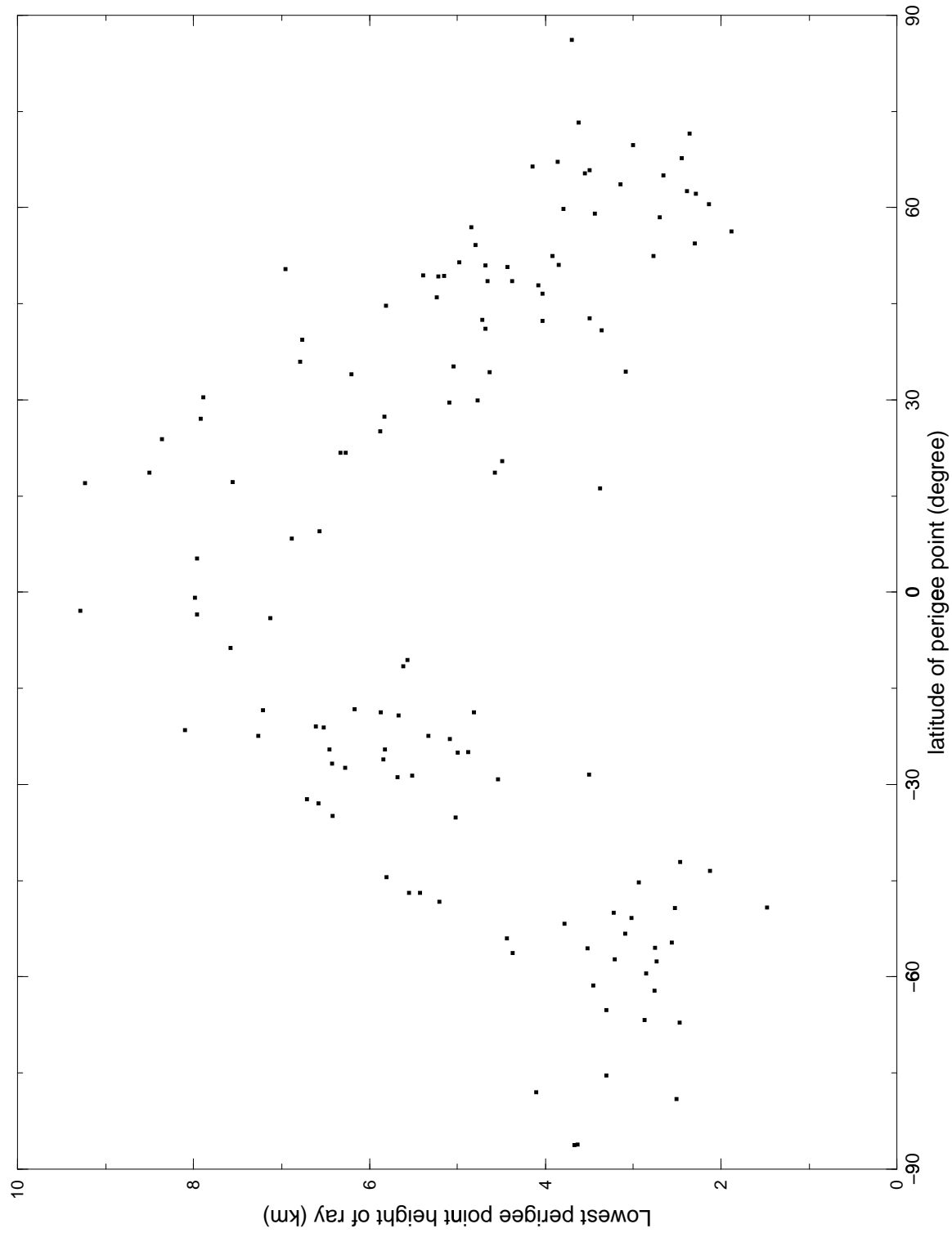


Fig. 11

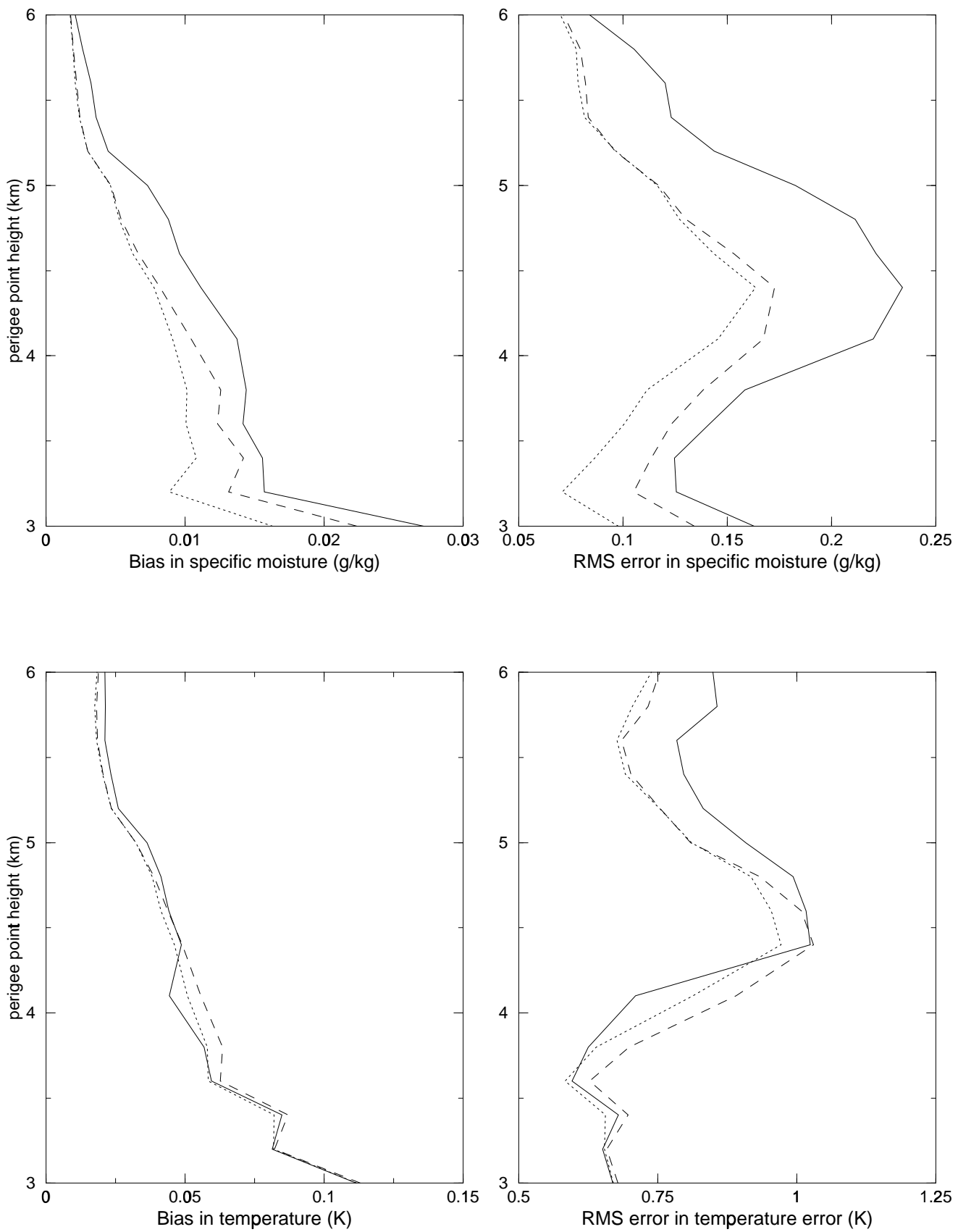


Fig. 12

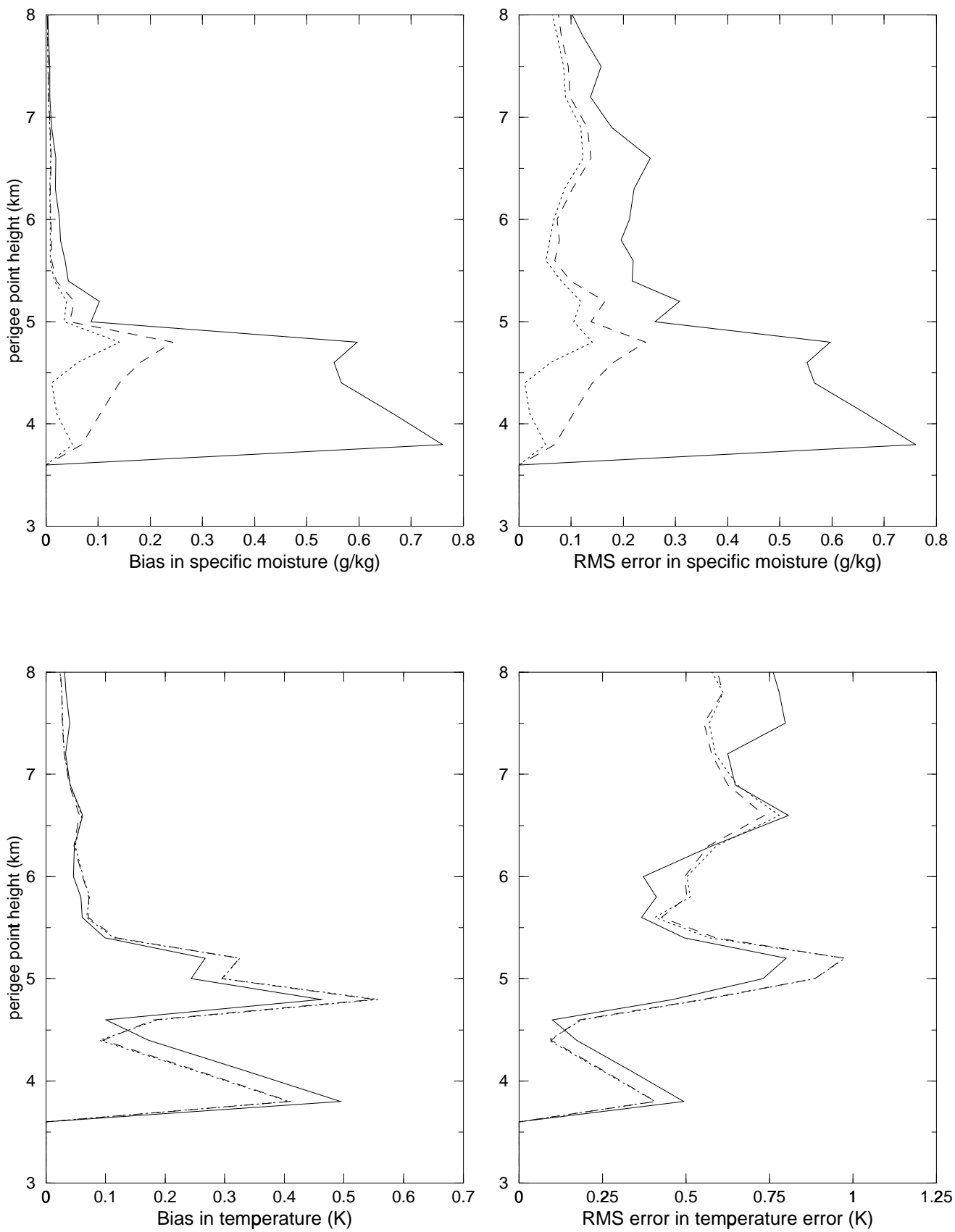


Fig. 13

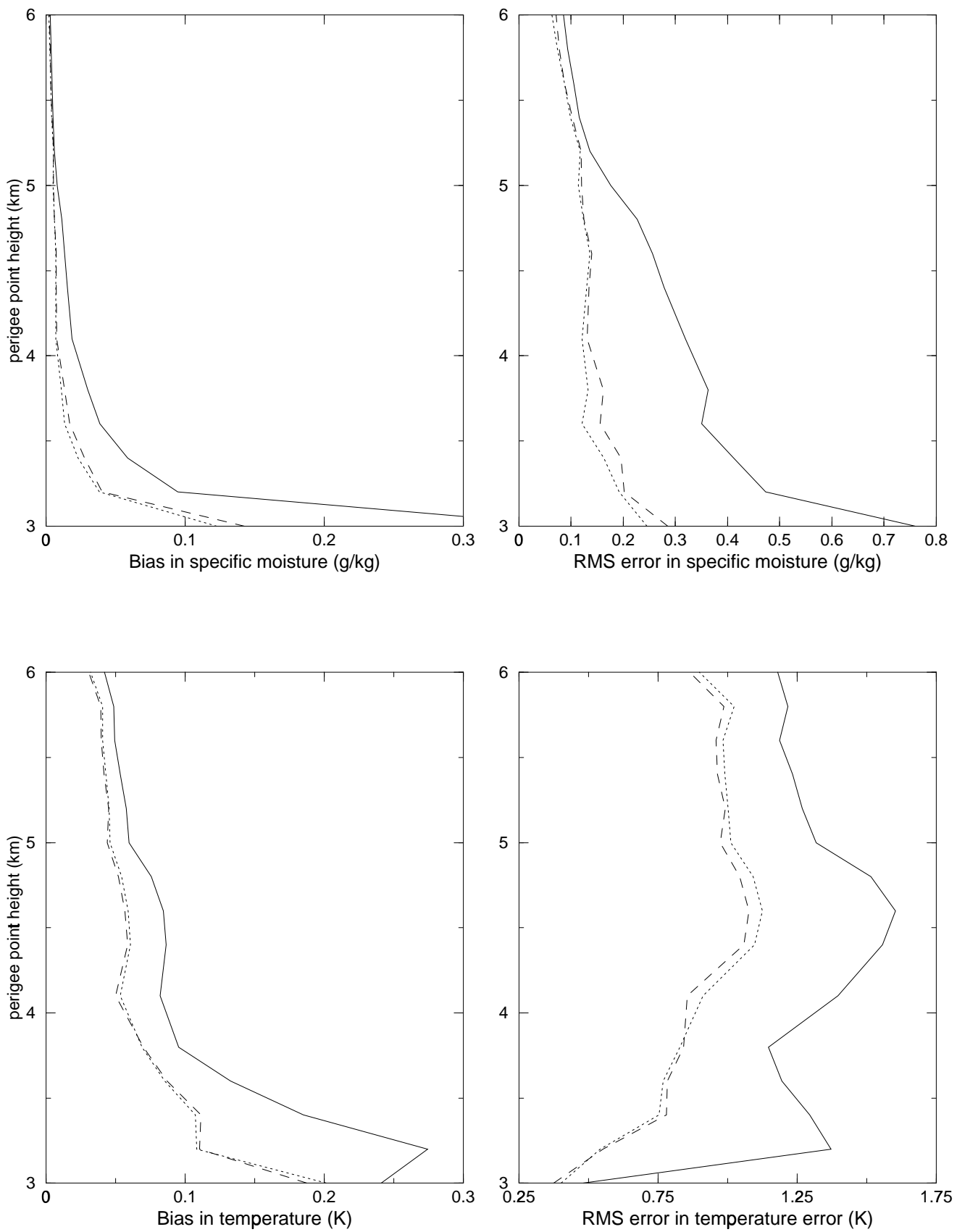


Fig. 14

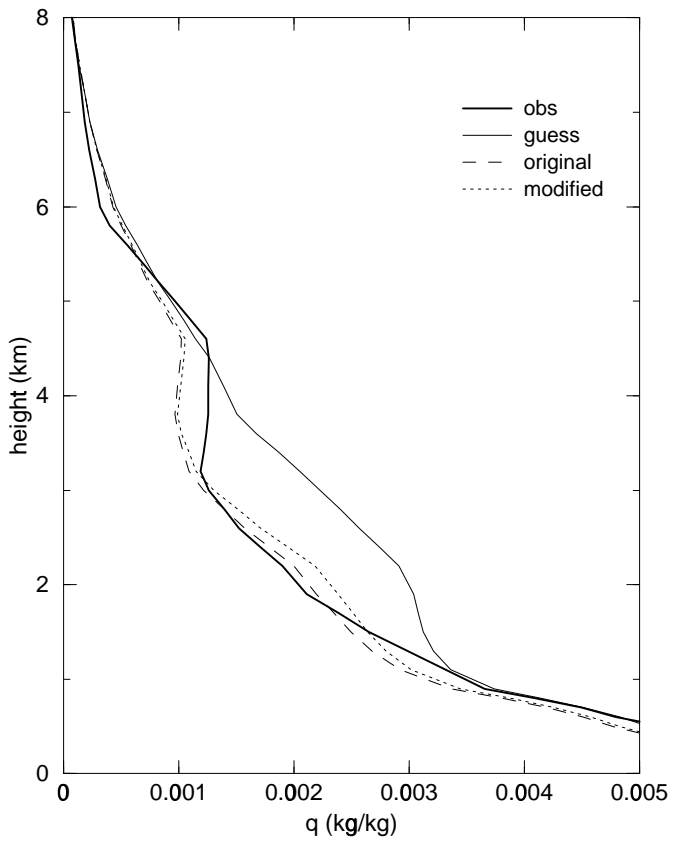
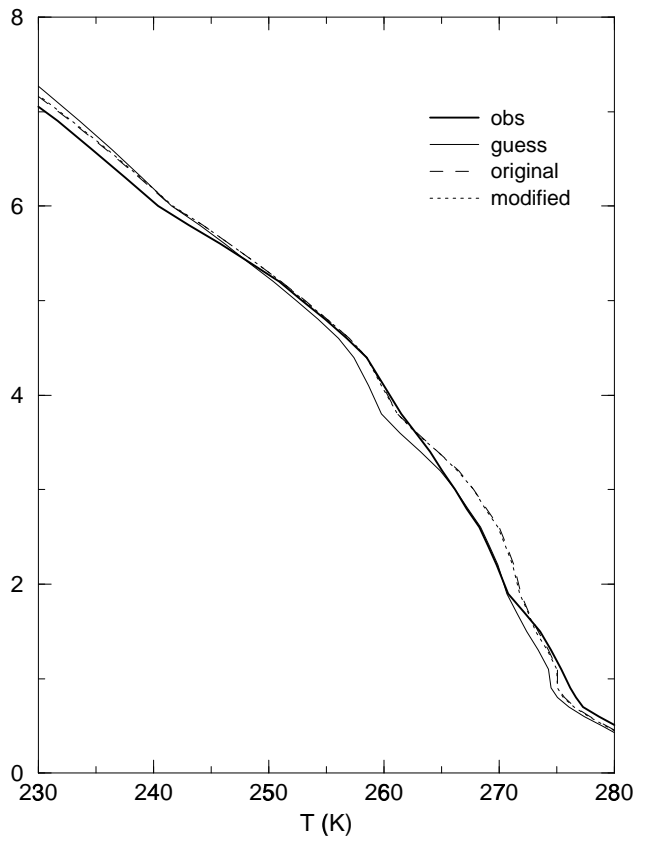
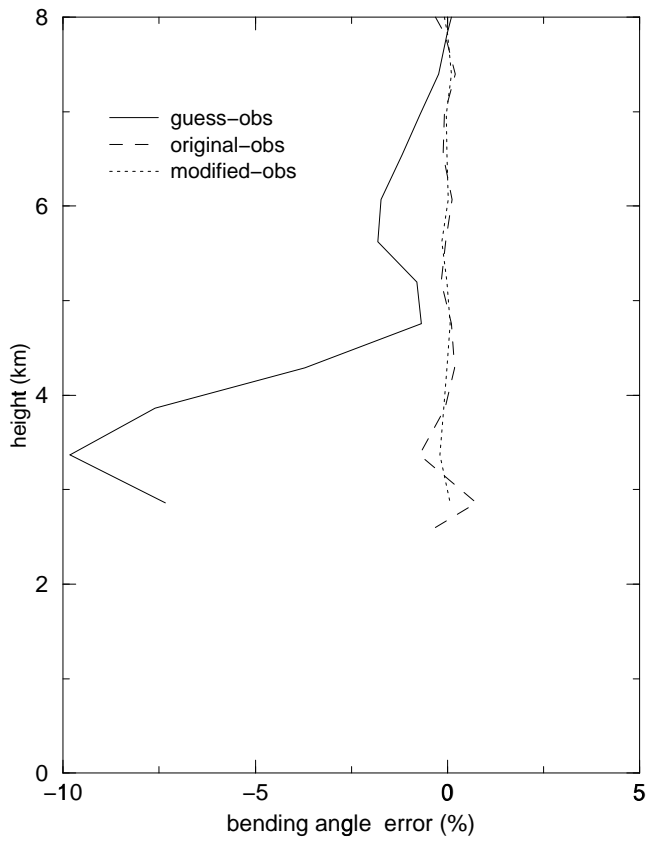


Fig. 15